Corrosion Science 180 (2021) 109188

Contents lists available at ScienceDirect

Corrosion Science

journal homepage: www.elsevier.com/locate/corsci

Inhibiting corrosion of aluminum alloy 5083 through *Vibrio* species biofilm

Yu Gao [a,b,1], Danqing Feng [c,1], Masoumeh Moradi [a,b,1], Chuntian Yang [a,b], Yuting Jin [a,b], Dan Liu [d], Dake Xu [a,b,*], Xiaobo Chen [e], Fuhui Wang [a,b]

[a] Shenyang National Laboratory for Materials Science, Northeastern University, Shenyang, 110819, China
[b] The State Key Laboratory of Rolling and Automation, Northeastern University, Shenyang, 110004, China
[c] State-Province Joint Engineering Laboratory of Marine Bioproducts and Technology, College of Ocean and Earth Sciences, Xiamen University, Xiamen, 361102, China
[d] School of Materials Science and Engineering, Hebei University of Science and Technology, Shijiazhuang, 050018, China
[e] School of Engineering, RMIT University, Carlton, VIC, 3053, Australia

ARTICLE INFO

Keywords:
A. Aluminum
B. SEM
B. EIS
B. Polarization
C. Microbiological corrosion
C. Neutral inhibition

ABSTRACT

Microbiologically influenced corrosion inhibition (MICI) of aluminum alloy (AA) 5083 by three representative *Vibrio* species were evaluated using electrochemical, surface analysis and surface characterization techniques. Interestingly, all the bacteria exhibited profound inhibitory effect on the corrosion of AA5083 in the chloride-containing culture medium. The MICI mechanism of tested *Vibrio* species is that mature biofilms acted as a diffusion barrier to prevent the penetration of corrosive chloride and consumed up the diffused oxygen by their aerobic respiration. Thus, the biofilm increased the passive range and inhibited the localized attack on the AA5083 surfaces.

1. Introduction

Biofilm, a community of one or more species of bacteria, always forms on the surface of metal and consequently leads to microbiologically influenced corrosion (MIC) [1–3]. MIC on steel, a key structural material in infrastructure, has been extensively explored in the presence of different aerobic and anaerobic bacteria [4–8]. However, studies on non-ferrous materials related MIC are rarely reported. Of those, light-weight aluminum alloys (AA) that are widely used for manufacturing of marine equipment are vulnerable to MIC. In general, AA exhibit a good corrosion resistance in mildly corrosive environment owing to the strong passivity derived from their native oxide layer upon the surface. However, they suffer from localized corrosion attack, in particular, in contact with marine environments [9–11]. In addition, the presence of a great number of microorganisms in seawater degrades the corrosion resistance of AA to some degree given some certain biological metabolism activities [12–14]. Sulfate-reducing bacteria (SRB), always blamed as a major culprit in MIC, caused a severe corrosion of AA5052 [15]. Smirnov et al. [16] also suggested that the main factor responsible for AA destruction by thirteen fungus and six bacterial species was the organic acids secreted in the course of bacterial metabolism.

In contrast, it is recognized that some biological activities of microorganisms contributed positively to the corrosion resistance of metal alloys, termed microbiologically influenced corrosion inhibition (MICI), since the first discovery by Pedersen et al. [17] in 1998. So far, the corrosion inhibitory effect of several bacterial species, such as *Pseudomonas flava, Pseudomonas stutzeri* [18], *Escherichia coli DH5α* [19], and even SRB [20] upon a number of ferrous and non-ferrous alloys have been reported. Different MICI mechanisms, including formation of a barrier film on metal surface [21], oxygen depletion [22], secreting inhibitory enzyme [23], and corrosion inhibition via biomineralization [24] have been proposed. Recently, Moradi et al. [25] have reported an excellent corrosion inhibitory effect of *Vibrio neocaledinocus* sp. which is comparative to that of metallic Ni coating, attracting the attentions to the *Vibrio* species. It is well known that biofilm is responsible for MIC and MICI [26]. *Vibrio* species are Gram-negative, motile with a curved rod shape, the most abundant bacteria in seawater, and they have strong ability to form biofilm on the metal surface. However, there is little known that how *Vibrio* species biofilms influence the corrosion process of the metal matrix where they attached. Thus, it is of great interest to figure out the potential dual roles, MIC or MICI, of different *Vibrio* species with the interactions of AA.

In this work, three representative *Vibrio* species, namely *Vibrio parahaemolyticus*, *Vibrio alginolyticus* and *Vibrio* sp. EF187016, were selected

* Corresponding author at: Shenyang National Laboratory for Materials Science, Northeastern University, Shenyang, 110819, China.
E-mail address: xudake@mail.neu.edu.cn (D. Xu).
[1] These authors contributed equally to this work.

https://doi.org/10.1016/j.corsci.2020.109188
Received 7 March 2020; Received in revised form 31 October 2020; Accepted 5 December 2020
Available online 30 December 2020

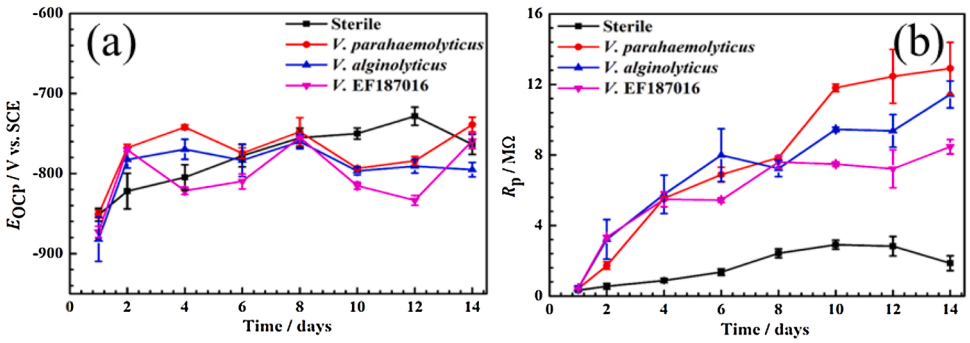

Fig. 1. Variations of (a) E_{OCP} and (b) R_P during the 14 days of incubation in different culture media.

and isolated from the East China Sea for revealing their corrosion inhibitory effect on AA5083 through electrochemical measurements and surface characterization.

2. Materials and methods

2.1. Microbiological culture and incubation

Three strains of marine *Vibrio* species were isolated from the East China Sea, Xiamen and identified as *V. parahaemolyticus*, *V. alginolyticus* and *V.* EF187016 by 16 s rRNA sequence. Sampling, strain isolation, and culture procedures have been described previously [27]. Bacteria were incubated in 2216E culture medium, composed of the following components (g/L): 19.45 NaCl, 5.98 $MgCl_2$, 3.24 Na_2SO_4, 1.80 $CaCl_2$, 0.55 KCl, 0.16 Na_2CO_3, 0.080 KBr, 0.034 $SrCl_2$, 0.080 $SrBr_2$, 0.022 H_3BO_3, 0.0040 Na_2SiO_3, 0.0024 NaF, 0.0016 NH_4NO_3, 0.0080 NaH_2PO_4, 5.0 peptone, 1.0 yeast extract and 0.10 ferric citrate. Initial pH of the culture medium was 7.6 ± 0.2. Before performing the experiment, the solution was sterilized in the autoclave at 121 °C for 20 min.

2.2. Materials

Square-shaped AA5083 specimens with dimensions of 10 mm × 10 mm × 5 mm were used in this study with a chemical composition (wt%) of Mg 4.36, Mn 0.50, Fe 0.16, Si 0.081, Cr 0.072, Cu 0.031, Ti 0.013, Zn 0.0025 and Al balance. Before measurements, all AA5083 coupons were mechanically ground with silicon carbide papers to surfaces finished of 1000 grit, ultrasonically rinsed with absolute ethanol for 15 min, dried and sterilized under ultraviolet radiation for 30 min.

2.3. Electrochemical tests

Electrochemical tests were performed with a three-electrode system in a quartz cell (250 mL) filled with 200 mL of culture medium as electrolyte. Electrical contact was provided to connect working electrode with others through a conductive copper wire (covered with insulate rubber) to the back side of specimens mounted in epoxy resin. The wires were then connected in such a way that only 1 cm^2 of each specimen was exposed. Platinum plate (10 mm × 10 mm × 1 mm) was used as counter electrode, and saturated calomel electrode (SCE) as reference electrode. Gamry electrochemical workstation (Reference 600, Inc, USA) was used to perform the electrochemical measurements, including open circuit potential (OCP), linear polarization resistance (LPR), electrochemical impedance spectroscopy (EIS) and potentiodynamic polarization curves. The potential was swept in the range from −5 mV to 5 mV (vs. E_{OCP}) at a scan rate of 0.125 mV/s for the LPR measurement. EIS tests were operated at stable open circuit potential (E_{OCP}), and the sinusoidal voltage was 5 mV at a frequency from 100 kHz to 0.01 Hz. EIS results were analyzed using ZSIMPWIN software (Princeton Applied Research, USA). Potentiodynamic polarization curves were recorded at a constant sweep rate of 0.166 mV/s. During the electrochemical measurements, the samples were immersed in a water bath to maintain the temperature at 30 °C. Three replicates were carried out for reproducibility. Current density variation of AA5083 as a function of time in sterilized abiotic and *Vibrio* species containing media was monitored with the same electrochemical workstation. Current density was recorded at a frequency of one reading per 10 s.

2.4. Immersion tests

Immersion tests were carried out in 100 mL conical flask. Three samples of AA5083 were put into 50 mL of sterile 2216E culture medium or inoculated medium with *Vibrio* species. The initial bacteria cell concentration in each conical flask was approximately 1.0 × 10^6 cells/mL. The conical flasks were incubated in 30 °C for 7 and 14 days, respectively.

2.5. Surface observation and characterization

Biofilms characteristics of different *Vibrio* species on AA5083 specimens were examined using field emission scanning electron microscopy (FESEM, Ultra Plus, Zeiss, Germany). Before biofilm observation, samples were removed from culture media and rinsed with phosphate buffered saline (PBS). The test coupons were fixed in 3% (v/v) glutaraldehyde solution for 4 h, and sequentially dehydrated with 50, 60, 70, 80, 90 and 100% ethanol (v/v) for 10 min at each concentration. Finally, the dehydrated samples were sputter coated with gold for FESEM observations.

Confocal laser scanning microscopy (CLSM, C2 Plus, Nikon, Japan) was also used for detecting live and dead sessile cells and biofilm morphology attached on the metal surface. The samples were cultivated with different *Vibrio* species for 7 and 14 days, respectively. After rinsing with PBS, they were stained with a mixture of fluorescent dyes (Live/Dead® BacLight™ Bacterial Viability Kit L7012, Life Technologies, Grand Island, NY, USA) according to the manufacturers' procedure. The excitation wavelengths of live cells were 488 nm and showed a green fluorescence while dead cells appeared red at an excitation wavelength of 559 nm, respectively [7].

To remove biofilm and examine corrosion morphology, procedures were taken according to the Chinese National Standards (CNS) GB/T 16545 − 1996. Briefly, samples were rinsed with distilled water, and then were exposed to 69.2 wt% nitric acid for 3 min to remove the corrosion products. Subsequently, the samples were ultrasonically cleaned using absolute ethanol. CLSM (LSM 710, Zeiss, Germany) was used to obtain the pits morphology.

X-ray photoelectron spectroscopy (XPS, Thermo VG, USA) analysis was used to evaluate the chemical composition of the corrosion products on the coupon surfaces after 14 days of exposure to the culture medium with and without *Vibrio* species. The XPS wide range was from 0 to 1350 eV. A monochromatic AI Kα X-ray source (1500 eV energy and 150 W power) was used within 50 eV pass energy and step size of 0.2 eV. The charge shifts were corrected using C 1s peak at 284.6 eV.

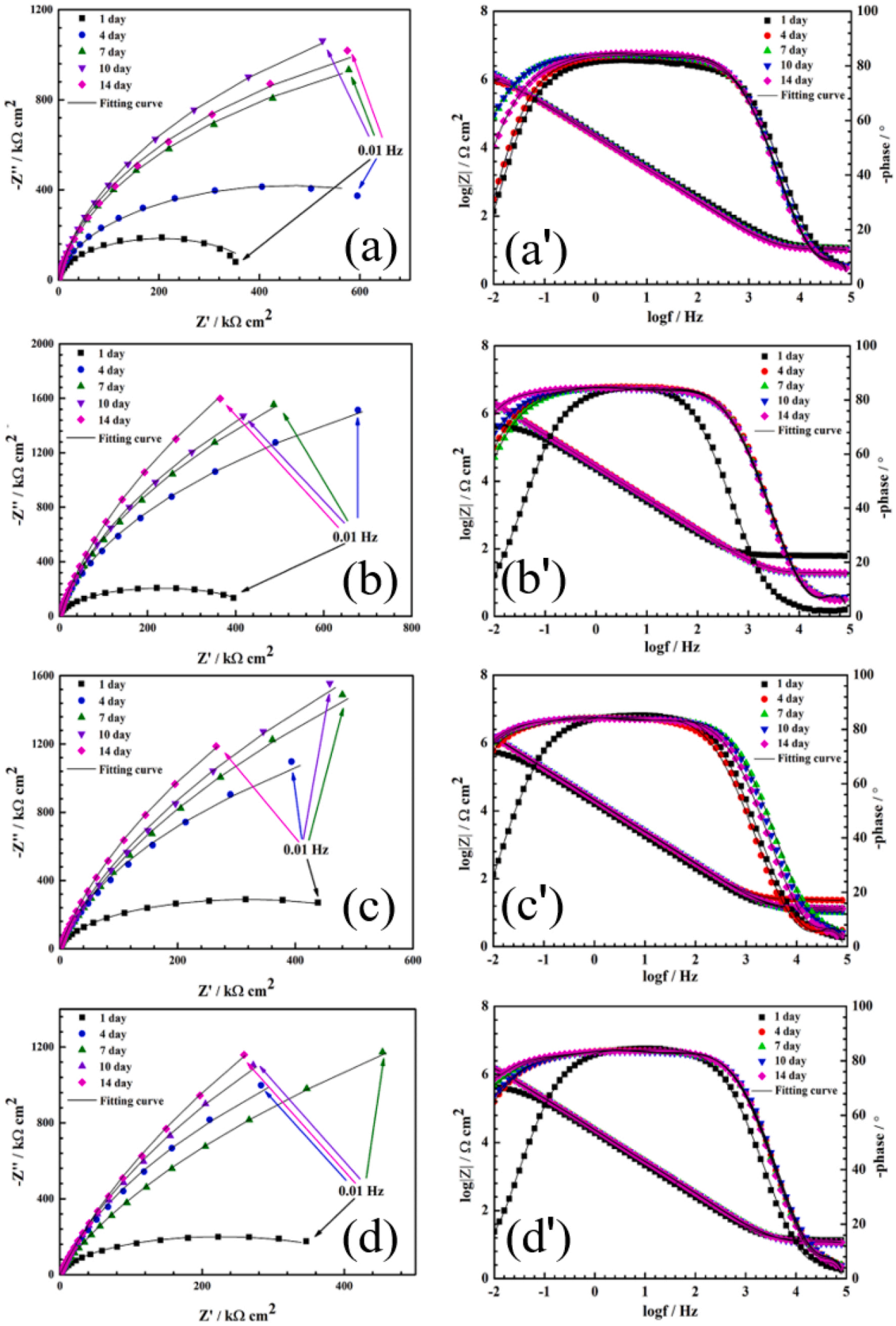

Fig. 2. The Bode and Nyquist plots of AA5083 coupons exposed to different media for different time: (a) (a') sterile medium, (b) (b') *V. parahaemolyticus*, (c) (c') *V. alginolyticus* and (d) (d') *V.* EF187016.

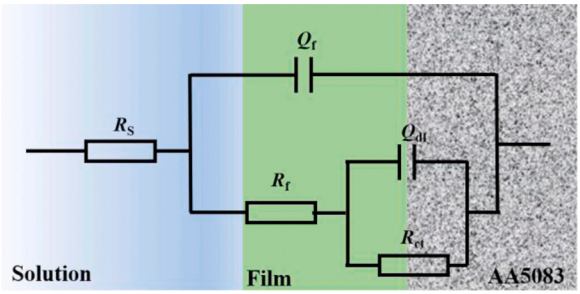

Fig. 3. Equivalent electrical circuit of AA5083 in different culture medium during 14-day incubation.

3. Results and discussion

3.1. Electrochemical tests

3.1.1. OCP and LPR

Fig. 1(a) shows the variations of E_{OCP} values of AA5083 specimens exposed to the sterile culture medium and inoculated medium with different *Vibrio* species for 14 days. In the sterile medium, E_{OCP} of AA5083 gradually shifted towards the positive direction due to the oxidation of AA5083 and formation of passive layer on the surfaces [28]. Besides, In the presence of *Vibrio* species, the metabolic activity of the bacteria and detachment-attachment cycle of the biofilm resulted in the significant fluctuation in E_{OCP} values [29].

The variations of LPR for AA5083 specimens during 14 days of exposure in the medium with and without *Vibrio* species are plotted in Fig. 1(b). It indicated that R_p values were almost stable with slight increments during exposure of 14 days in the sterile medium. In the presence of *Vibrio* species, R_p increased dramatically on the second day and the resistance values were obviously higher than that in the sterile medium. The R_p values were in the ranking of *V. parahaemolyticus* > *V. alginolyticus* > *V.* EF187016 > sterile medium over time. Moradi et al. [25] reported that the inhibitory effect of *Vibrio neocaledonicus* sp. was observed after one hour of exposure due to the oxygen depletion. But in this work, all three *Vibrio* species showed their first inhibitory effect after 1 day when the biofilm already formed on the AA5083 surfaces. The possible reason to explain this phenomenon is that *V. neocaledonicus* sp. mainly relied on its strong oxygen depletion ability, by which it can consume the diffused oxygen in a very quick manner, leading to the corrosion prevention. While the *Vibrio* species tested in this work started to show their MICI effect after their biofilms were fully formatted, which also acted as a diffusion barrier to prevent the penetration of the corrosive agents such as chloride ions.

3.1.2. EIS

Nyquist and Bode plots of all samples after exposure in 2216E medium with and without *Vibrio* species for 1, 4, 7, 10 and 14 days are depicted in Fig. 2. The semicircle diameter of Nyquist plots (Fig. 2(a–d)) was obviously larger in the biotic medium than that of the abiotic control at each time point, reflecting that *Vibrio* species enhanced the corrosion resistances of AA5083. And a significant increased trend of impedance magnitude was also found in the biotic medium, which can be attributed to the biofilm formation and maturation on AA5083 surfaces during 14 days. The biofilm was supposed to act as a physical barrier and inhibit the penetration and diffusion of aggressive ions to AA5083 surfaces over the exposure time [23].

Bode-phase plots in Fig. 2(a'–d') show a broad time constant joined by two-time constants for all the systems. The one in high frequencies could be attributed to a surface oxide layer and the formation of corrosion products on the metal surface, while the other one in low frequencies may be caused by the electric double layer, and the conjunction of the time constants indicated that the frequency responsed of these time constants were similar. For *Vibrio* species - containing medium, the capacitive behavior of the passive film at the low frequency zone can be attributed to the cumulative capacitive effect resulted from the formation of a biofilm [30]. In contrast, in the sterile medium, the

Table 1
EIS fitting results of AA5083 coupons with and without *Vibrio* species in 2216E medium.

Duration/ day	R_s/Ω cm^2	Q_f		R_f/ Ω cm^2	Q_{dl}		R_{ct}/ Ω cm^2	$\Sigma\chi^2$
		Y_f/ $\Omega^{-1}s^n$ cm^2	n_f		Y_{dl}/ $\Omega^{-1}s^n$ cm^2	n_{dl}		
Sterile								
1	10.6	6.4×10^{-6}	0.8	3.2×10^{5}	7.4×10^{-6}	0.9	4.7×10^{5}	2.8×10^{-4}
4	8.4	7.0×10^{-6}	0.9	3.7×10^{5}	6.1×10^{-6}	0.9	1.3×10^{6}	5.1×10^{-5}
7	10.7	7.3×10^{-6}	0.8	2.7×10^{5}	5.5×10^{-6}	0.9	2.2×10^{6}	1.6×10^{-4}
10	11.0	7.3×10^{-6}	0.9	4.7×10^{5}	5.7×10^{-6}	0.9	3.5×10^{6}	2.4×10^{-5}
14	10.1	5.1×10^{-6}	0.9	4.7×10^{5}	7.8×10^{-6}	0.9	3.4×10^{6}	5.7×10^{-5}
V. parahaemolyticus								
1	13.8	6.6×10^{-6}	0.9	1.5×10^{5}	3.9×10^{-6}	0.9	5.2×10^{5}	4.1×10^{-5}
4	12.3	5.4×10^{-6}	0.9	5.7×10^{5}	3.3×10^{-6}	0.9	4.5×10^{6}	5.9×10^{-5}
7	13.3	2.2×10^{-6}	0.9	7.2×10^{5}	3.1×10^{-6}	0.9	6.7×10^{6}	5.4×10^{-5}
10	12.8	4.2×10^{-6}	0.8	7.8×10^{5}	3.4×10^{-6}	0.9	8.9×10^{6}	3.6×10^{-5}
14	12.4	1.2×10^{-6}	0.9	8.2×10^{5}	2.6×10^{-6}	0.9	1.3×10^{7}	6.4×10^{-5}
V. alginolyticus								
1	13.6	3.8×10^{-6}	0.9	1.4×10^{5}	5.4×10^{-6}	0.9	6.4×10^{5}	1.2×10^{-4}
4	10.6	3.2×10^{-6}	0.9	4.1×10^{5}	5.5×10^{-6}	0.9	4.6×10^{6}	7.4×10^{-5}
7	13.8	5.0×10^{-6}	0.9	5.6×10^{5}	4.7×10^{-6}	0.9	5.9×10^{6}	3.4×10^{-5}
10	8.4	2.0×10^{-6}	0.9	6.2×10^{5}	4.3×10^{-6}	0.9	6.0×10^{6}	1.4×10^{-4}
14	10.0	5.8×10^{-6}	0.9	7.1×10^{5}	4.1×10^{-6}	0.9	1.1×10^{7}	1.9×10^{-5}
***V.* EF187016**								
1	10.6	4.1×10^{-6}	0.9	1.2×10^{5}	6.3×10^{-6}	0.9	5.1×10^{5}	1.1×10^{-4}
4	11.2	3.4×10^{-6}	0.9	4.0×10^{5}	5.7×10^{-6}	0.9	4.9×10^{6}	4.1×10^{-5}
7	12.6	0.8×10^{-6}	0.9	5.1×10^{5}	6.0×10^{-6}	0.9	4.4×10^{6}	5.5×10^{-5}
10	10.7	9.8×10^{-6}	0.9	6.0×10^{5}	5.7×10^{-6}	0.9	5.7×10^{6}	7.0×10^{-5}
14	9.5	2.1×10^{-6}	0.8	6.6×10^{5}	4.3×10^{-6}	0.9	8.2×10^{6}	1.1×10^{-4}

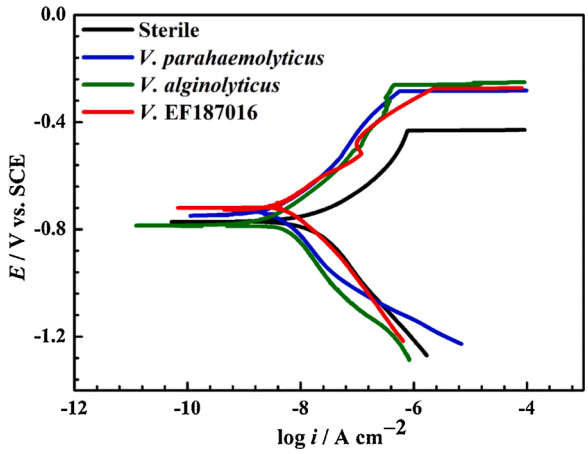

Fig. 4. The polarization curves of AA5083 coupons after 14 days in the sterile medium and in the presence of *V. parahaemolyticus*, *V. alginolyticus* and *V.* EF187016.

resistive behavior was observed in all the range of frequency regions. Additionally, it can be observed that in the medium with *Vibrio* species, the abovementioned two time constants appeared at lower frequencies, indicating a slower corrosion reaction rates [31].

The EIS curves were fitted according to the proposed equivalent circuit as shown in Fig. 3, and all the obtained chi-squared (χ^2) values were below 10^{-4}. R_s, R_{ct} and R_f represent the solution resistance, charge transfer resistance and film resistance, respectively. It is necessary to use constant phase element (Q) instead of an ideal capacitance on account of the diffusion effect of the heterogeneity caused by electrode corrosion in the medium [30]. So Q_f and Q_{dl} are film capacitance and double layer capacitance, respectively. The impedance of CPE was evaluated from Eq. (1):

$$Z_{CPE} = \left({}^{1}/_{Y_0}\right)(j\omega)^{-n} \quad (1)$$

Where Y_0 is the CPE parameter, j is the imaginary number, ω is the angular frequency and n is the CPE exponent (n and Y_0 represent the quantity of surface inhomogeneity and the magnitude of admittance of the CPE) [32].

As shown in the equivalent circuit (Fig. 3), (R_fQ_f) represents the external characteristics of the membrane layer, and ($R_{ct}Q_{dl}$) represents the interface features. In Table 1, the Q_{dl} values for describing the capacitance of the double layer in the biotic systems were lower than those in the sterile system, confirming the decrease of electrical conductivity [33]. The R_{ct} values in the presence of different *Vibrio* species were much higher than those of the sterile medium, indicating higher corrosion resistance of AA5083 caused by the bacteria. The highest R_{ct} of 1.3×10^7 Ω cm^2 during the incubation of 14 days was observed for *V. parahaemolyticus*. The other two *Vibrio* species, *V. alginolyticus* and *V.* EF187016, showed a similar trend and the R_{ct} values reached 1.1×10^7 Ω cm^2 and 8.2×10^6 Ω cm^2 after 14 days, respectively. In addition, R_f and Q_f values revealed the characteristics of the metal surface film. Compared to the sterile medium, the Q_f values were obviously decreased, indicating the increase of film thickness. The adsorption of the inhibited film on the metal surfaces lead to the decline of conductivity and the augment of R_f. Moreover, in the presence of *Vibrio* species, R_f values increased and Q_f values decreased over time, demonstrating that the film layer gradually thickened and the protective effect enhanced. The order of the obtained maximum R_f was as follows: *V. parahaemolyticus* > *V. alginolyticus* > *V.* EF187016. The trend of R_f may be related to the thickness of biofilm covered on the AA5083 surfaces. The above data further indicated that the combination of biofilm and oxide film improved the densification of the surface film layer, and the substances secreted by microorganisms modified the membrane/metal interface and increased the protective effect of the oxide layer [34,35]. The biofilm can serve with the oxide layer as an intact protective film.

Table 2
Corrosion parameters from the polarization curves for AA5083 coupons.

Sample	E_{corr}/V vs. SCE	i_{corr}/nA cm^{-2}	E_{pit}/V vs. SCE	Inhibition rate
Sterile	−0.76 ± 0.12	25.47 ± 6.99	−0.40 ± 0.05	
V. parahaemolyticus	−0.84 ± 0.08	4.42 ± 0.88	−0.28 ± 0.00	69.11 %
V. alginolyticus	−0.83 ± 0.06	4.87 ± 0.64	−0.30 ± 0.12	59.91 %
V. EF187016	−0.81 ± 0.04	7.65 ± 0.69	−0.31 ± 0.04	53.44 %

3.1.3. Potentiodynamic polarization curve

Fig. 4 shows the potentiodynamic polarization curves for AA5083 samples after 14 days of exposure to the sterile medium and the medium incubated with different *Vibrio* species. The corresponding Tafel analysis results are listed in Table 2. The estimated corrosion current density through Tafel fitting also demonstrated that i_{corr} of AA5083 reduced approximately 5 folds in the presence of *V. parahaemolyticus* (4.42 nA cm^{-2}) and *V. alginolyticus* (4.87 nA cm^{-2}), while 3.33 folds in the presence of *V.* EF187016 (7.65 nA cm^{-2}) compared to that of the sterile medium (25.47 nA cm^{-2}).

Pitting is always detrimental to AA in marine environments due to the penetration of chloride ions into the oxide layers [10]. According to the polarization curves, the pitting potential (E_{pit}) shifted positively in the presences of all three *Vibrio* species, reflecting a better pitting corrosion resistance of AA5083. As shown in Fig. 4, the *Vibrio* species biofilm inhibited the kinetics of anodic reaction, slowed down the corrosion rate and increased the passivity of the AA5083. In addition, the presence of *Vibrio* species (specially *V. parahaemolyticus* and *V. alginolyticus*) also resulted in a small shift of the cathodic branch of the polarization curves leftward, showing the inhibiting effect of the cathodic reaction.

3.2. Surface morphology analysis

Fig. 5 shows the FESEM images of AA5083 surfaces after exposure in the culture medium inoculated with *V. parahaemolyticus* (a, a'), *V. alginolyticus* (b, b') and *V.* EF187016 (c, c') for 7 and 14 days, respectively. After 7 days, a heterogenous biofilm was covered on the AA5083 surfaces. The thickness and surface area of biofilm were increased over the exposure time, and a thicker and more uniform biofilm was observed on the AA5083 surfaces in the presence of *Vibrio* species.

Pitting morphology of the AA5083 surfaces immersed in the sterile medium and medium inoculated with different *Vibrio* species for 14 days was examined by CLSM as shown in Fig. 6. The maximum pit depth was determined by averaging the deepest 10 pits from each coupon surface (total of three coupons). The maximum pit depth on AA5083 exposed in the sterile medium was 5.4 μm. Pitting corrosion was also observed in the presence of *Vibrio* species, however, the pit depth and width were much smaller than those observed in the sterile medium as shown in Fig.7. For shallow pits, the activation energy for re-passivation required is less than deeper pits. Therefore, the shallow pits in the presence of biofilm may re-passivate faster, adhesion of biofilm enhancing the pitting corrosion resistance [36].

Moreover, the average maximum pit depth and pit density are listed in Table 3. Compared with the data in the abiotic medium, the *Vibrio* species significantly decreased the pit depth and pit density. Especially in the presence of *V. parahaemolyticus*, the average maximum pit depth

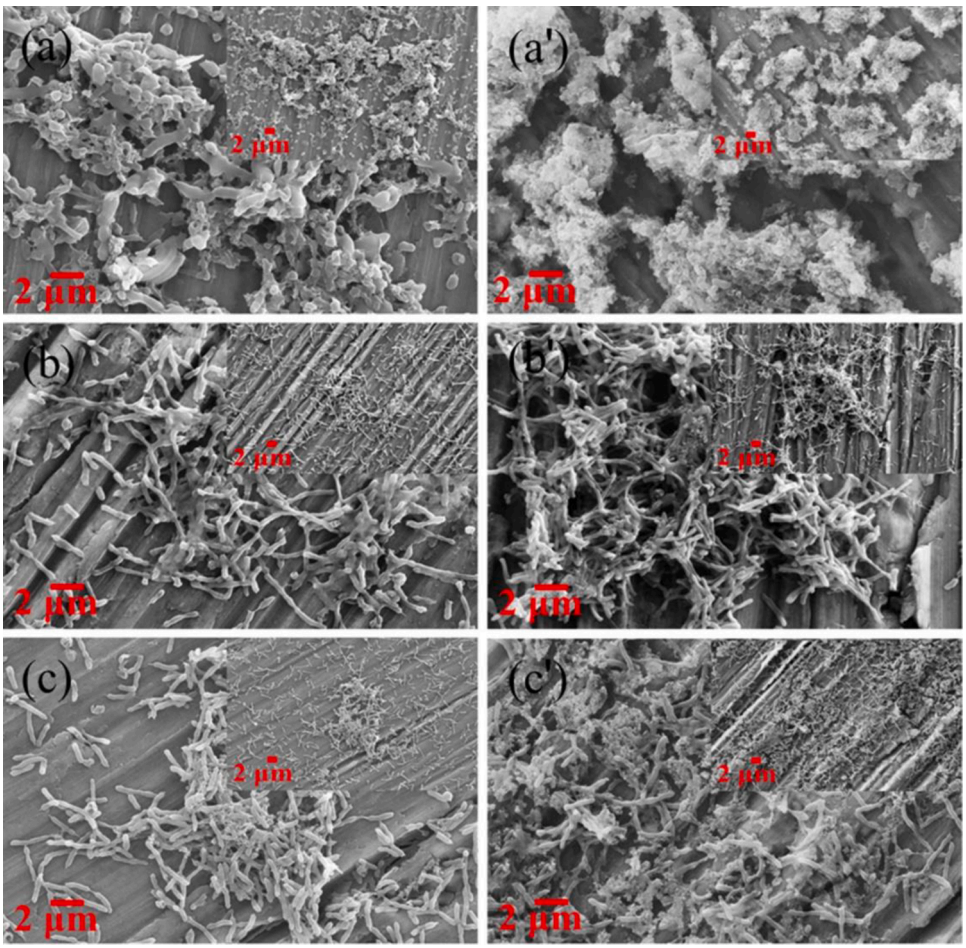

Fig. 5. FESEM images of biofilm formed on AA5083 coupon surfaces for 7 days and 14 days after exposure to (a) (a') *V. parahaemolyticus*, (b) (b') *V. alginolyticus* and (c) (c') *V.* EF187016.

reduced to 2.0 μm and the number of pits was only 117/cm^2. The 2216E culture medium is composed of approximately 2% NaCl, which causes the pitting on AA5083 surfaces. The above results demonstrated the ability of *Vibrio* species for preventing the pitting corrosion by hindering the penetration of chloride ions. These results made a good agreement with the electrochemical results above.

Pitting of AA5083 is a very complex process that can be affected by various factors [10]. The pH of the solution was measured during 14 days of exposure in Fig. 8(a). All three *Vibrio* species could increase the solution pH, indicating that the bacterial metabolic activity didn't have any acidic attack on the surface and the pitting was only caused by the penetration of chloride ions on AA5083 surfaces.

3.3. Surface characterization

Fig. 8(b) represents the broad XPS survey spectra of AA5083 specimens exposed to the sterile medium and medium inoculated with different *Vibrio* species for 14 days. The main elements (Al 2p, Mg 1s, Ca 1s, Na 1s, Cl 1s, C 1s, N 1s and O 1s) on the surfaces of AA5083 are listed in Table 4. The presence of C, N and O elements in the sterile medium was caused by the adsorption of organic macromolecules in the culture medium [14]. The higher concentration of C, N and O elements in the inoculated medium was attributed to the biofilm formation on the metal surfaces.

To better understanding the composition of the corrosion products on the coupon surfaces, Al 2p core-level spectra of the coupon surfaces weas conducted (Fig. 8c–f). The core-level Al 2p spectrum could be deconstructed into two peaks at binding energy values of 72.5 and 74.6 eV corresponding to the presence of Al and Al_2O_3 in the sterile medium. In the presence of *Vibrio* species, the Al peak disappeared, and $Al(OH)_3$ was detected in addition to Al_2O_3. The *Vibrio* species changed the type of oxide layer on the AA5083 surfaces by affecting the solution pH. It is well known that both Al_2O_3 and $Al(OH)_3$ are amorphous, and $Al(OH)_3$ can decompose to Al_2O_3 by releasing water [37]. So, the changed oxide layer of AA5083 was not the main reason to improve the corrosion resistance in the presence of chloride ions.

3.4. Biofilm observation

To understand the corrosion inhibitory mechanism of *Vibrio* species on AA5083, the biofilm structure and thickness were examined using CLSM. As shown in Fig. 9, all three species formed a compact biofilm which covered almost the whole surfaces of AA5083 after 7 days of exposure. The average biofilm thickness calculated from the largest three biofilm thickness after 7 days was 39.2 ± 3.9 μm, 32.0 ± 2.7 μm and 28.5 ± 4.5 μm for *V. parahaemolyticus*, *V. alginolyticus* and *V.* EF187016, respectively. And the thickness increased to 48.8 ± 1.8 μm, 39.1 ± 2.2 μm and 35.0 ± 3.7 μm after incubation of 14 days in the culture medium containing *V. parahaemolyticus*, *V. alginolyticus* and *V.* EF187016, respectively. The biofilm thickness data exhibited a good agreement with R_f values obtained from EIS results, while R_f and biofilm thickness showed the same ranking of *V. parahaemolyticus* > *V. alginolyticus* > *V.* EF187016. Herein, it can be concluded that the mature biofilm enhanced the corrosion resistance of AA5083.

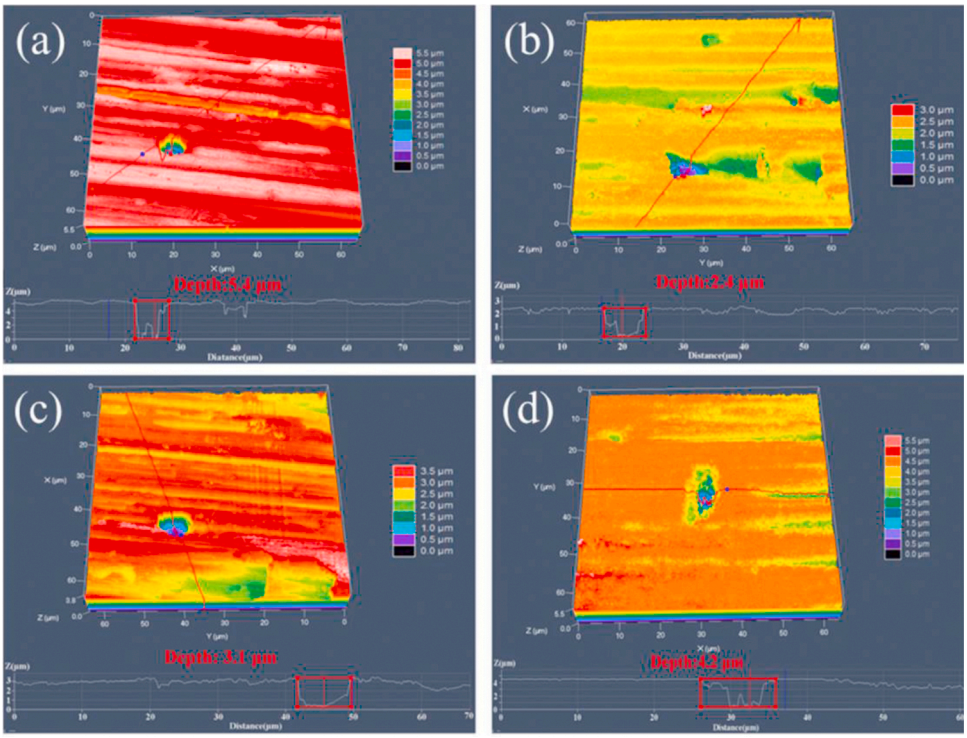

Fig. 6. 3D CLSM images of the maximum pit depth on coupon surfaces after 14 days: (a) sterile medium, (b) *V. parahaemolyticus*, (c) *V. alginolyticus* and (d) *V.* EF187016.

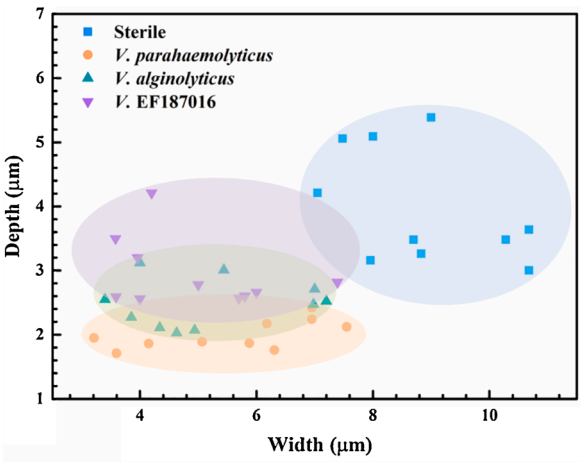

Fig. 7. Depth and width of the deepest pits observed on AA5083 coupon surfaces in the presence and absence of *Vibrio* sp. biofilm after immersion for 14 days.

Table 3
The average maximum pit depth and pit density on the coupon surfaces after 14 days.

Sample	Average maximum pit depth (μm)	Pit density (1/cm^2)
Sterile	4.0 ± 0.8	266 ± 44
V. parahaemolyticus	2.0 ± 0.2	117 ± 14
V. alginolyticus	2.5 ± 0.3	167 ± 6
V. EF187016	2.9 ± 0.5	177 ± 12

3.5. The inhibitory mechanism of Vibriospecies on AA5083 surfaces

V. parahaemolyticus was selected for the further investigation of its corrosion inhibitory mechanism of AA5083 because of its highest inhibitory effect (69.11%). The attachment of sessile bacteria cells and their metabolites on the AA5083 surfaces were stained and observed after 12 and 24 h using CLSM according to the previously reported procedures [6]. In Fig. 10(a), blue, red and green represent the sessile cells, proteins, and polysaccharides respectively. After incubation of 12 h, there was a large quantity of proteins and bacterial cells attached to the surfaces. After 24 h of exposure (Fig. 10b), the biofilm grew more mature, the protein and sessile cells were increased on the AA5083 surfaces. The sessile cells occupied the bottom layer of the biofilm, and they were covered with proteins (dominant red color). However, only a small amount of polysaccharide was found on the surfaces. The variation of current versus time was measured after 1 and 7 days as shown in Fig. 10(c) and (d), the cathodic current of AA5083 in the presence of *V. parahaemolyticus* was much lower than that in the sterile medium, approving the corrosion inhibitory efficiency of the biofilm. The irreversible attachment stage always lasts up to 24 h, which is the second stage for biofilm formation [38]. The above data indicated that *V. parahaemolyticus* biofilm started to inhibit corrosion when irreversible attachment was achieved. When the matured biofilm was formed on the AA5083 surfaces after 7 days as shown in Fig. 9, the cathodic current shifted more negatively, indicating a better inhibitory efficiency with thicker and more mature biofilm. The above data indicated that the irreversible attachment of the *V. parahaemolyticus* started to inhibit the corrosion of AA5083, while mature biofilm showed much better inhibitory effect. The thicker biofilm may act as a better diffusion barrier against the penetration of aggressive ions, resulting in decreased corrosion rate and risk of localized attack.

It is well known that *Vibrio* species are able to respire oxygen in aerobic environment, which is always a strong electron acceptor and corrosive agent [39]. Thus, the *Vibrio* species consumed up the oxygen underneath the biofilm, which provided a local anerobic environment

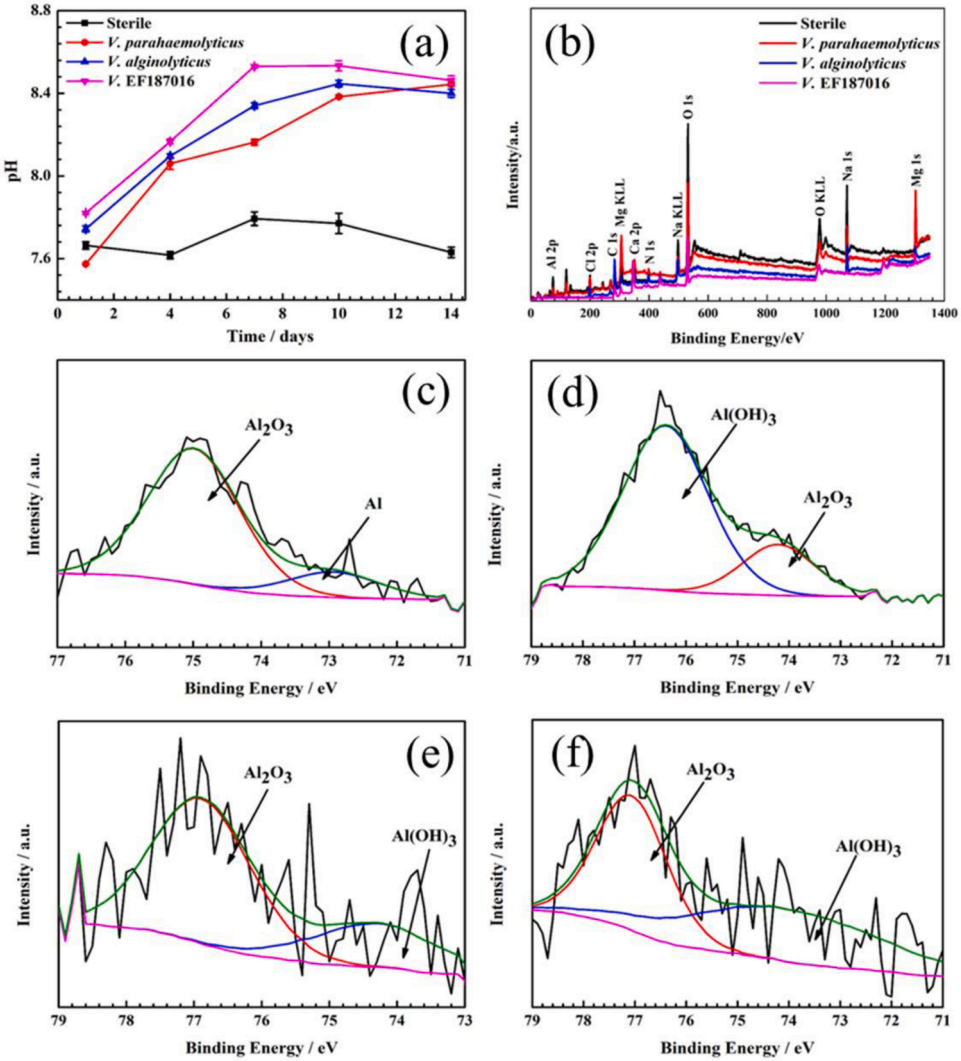

Fig. 8. Variation of pH and XPS spectra of AA5083 coupons in different media for 14 days: (a) pH, (b) wide XPS spectra and spectra of Al 2p: (c) sterile medium, (d) *V. parahaemolyticus*, (e) *V. alginolyticus* and (f) *V.* EF187016.

Table 4
Surface element contents of AA5083 coupons measured by XPS.

Atomic percent (%)	Al	Mg	Ca	Na	Cl	C	N	O
Sterile	28.7	1.9	3.7	5.7	7.3	7.1	0.4	45.2
V. parahaemolyticus	3.2	1.6	1.6	0.7	5.6	54.4	7.3	25.6
V. alginolyticus	1.2	2.2	7.0	4.3	6.8	54.6	6.7	17.2
V. EF187016	4.7	1.8	17.6	1.8	2.1	29.1	2.7	40.2

and facilitated the protection of the AA5083 from corrosion caused by the oxygen attack. It is previously reported that *V. neocaledonicus* sp. prevented the corrosion of carbon steel by depletion of oxygen [25]. Here, *V. parahaemolyticus* decreased the cathodic reaction which was closely related to the oxygen reduction. The biofilm can also prevent the diffusion of chloride ions to the coupon surface, achieving the protection of AA5083 matrix. The proposed corrosion inhibition mechanism by the *Vibrio* species was illustrated in Fig. 11.

4. Conclusions

In this work, MICI of AA5083 was investigated in the presence of three representative *Vibrio* species biofilm. All three *Vibrio* species showed the inhibitory effect against the corrosion of AA5083. *Vibrio* species biofilm decreased the corrosion current density and inhibited the pitting corrosion of AA5083. Based on surface analysis, thick and homogenous biofilm was formed by *Vibrio* species on the AA5083 surfaces. The biofilm behaved as a protective layer against the diffusion of corrosive ions and consumed of the oxygen according to the electrochemical results. In addition, their inhibition efficiency increased over the exposure time as the biofilm matured and reached in 69.11% for *V. parahaemolyticus*, 59.91% for *V. alginolyticus* and 53.44% for *V.* EF187016 after 14 days. Our work provides a new insight into the MICI mechanism of AA from the perspective of biofilm protection. The *Vibrio* biofilm possess the potential to be a corrosion protection "material" in marine environment.

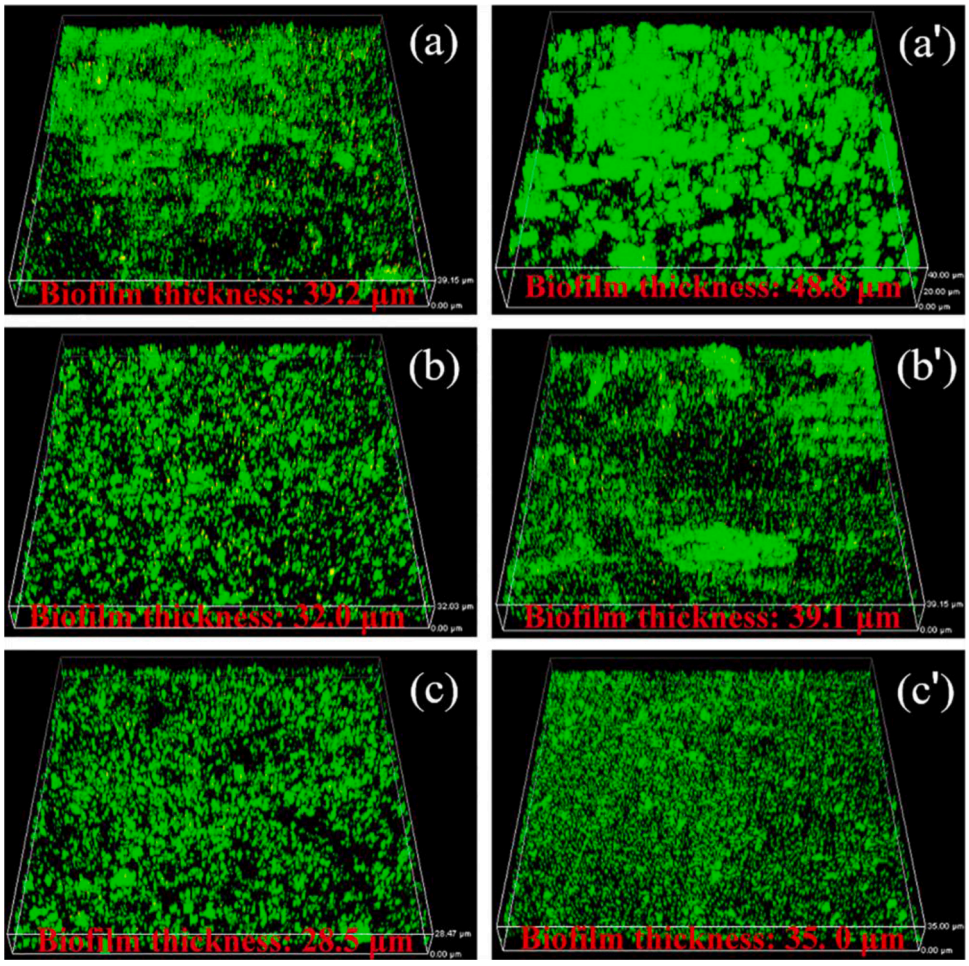

Fig. 9. 3D CLSM images of AA5083 coupons in the presence of (a) (a') *V. parahaemolyticus*, (b) (b') *V. alginolyticus* and (c) (c') *V.* EF187016 after 7 days and 14 days immersion.

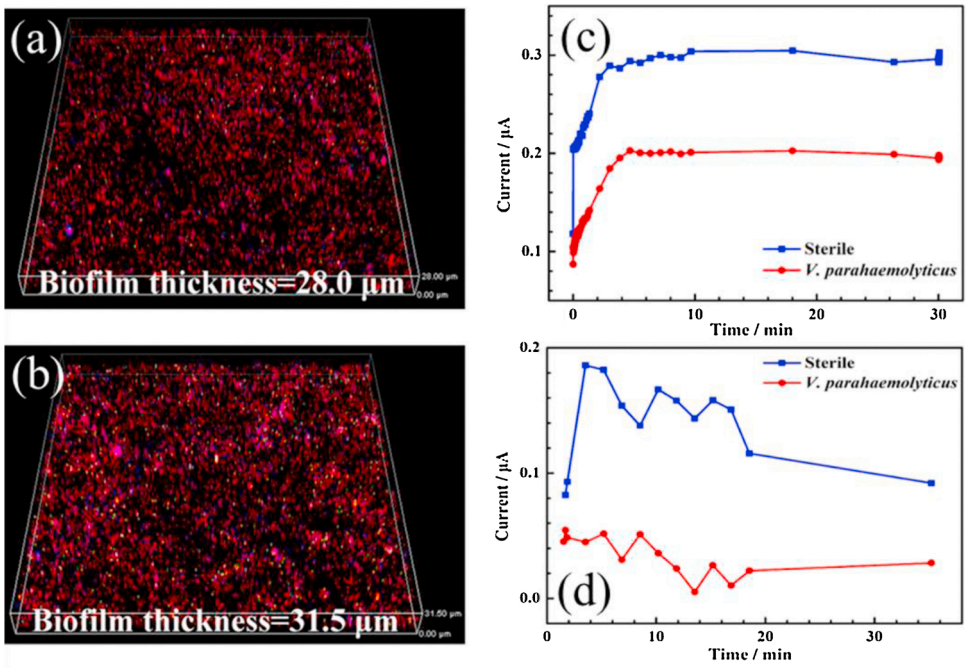

Fig. 10. 3D CLSM images and corrosion current of AA5083: 3D CLSM images of *V. parahaemolyticus* biofilms after (a) 12 h and (b) 24 h, corrosion current in sterile medium and in the presence of *V. parahaemolyticus* after (c) 1 day and (d) 7 days.

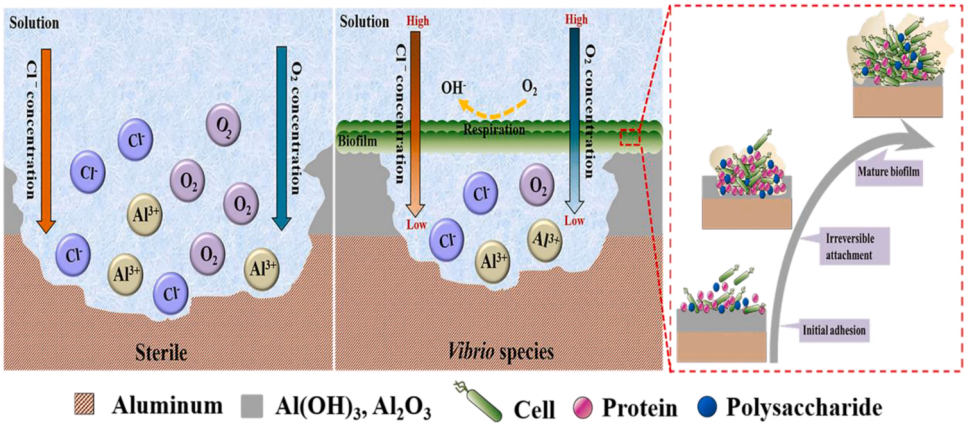

Fig. 11. Schematic illustration of the proposed MICI mechanism of AA5083.

CRediT authorship contribution statement

Yu Gao: Conceptualization, Data curation. **Danqing Feng:** Funding acquisition, Investigation. **Masoumeh Moradi:** Funding acquisition, Investigation. **Chuntian Yang:** Project administration. **Yuting Jin:** Project administration. **Dan Liu:** Formal analysis. **Dake Xu:** Supervision. **Xiaobo Chen:** Resources. **Fuhui Wang:** Resources.

Declaration of Competing Interest

The authors report no declarations of interest.

Acknowledgements

This work is financially supported by the National Natural Science Foundation of China (Nos. U2006219 and 51871050), the Natural Science Foundation of Liaoning Province (No. 20180510041), the Liaoning Revitalization Talents Program (No. XLYC1907158) and the Fundamental Research Funds for the Central Universities of the Ministry of Education of China (N180205021, N180203019, N2002019).

References

[1] P.J. Antony, S. Chongdar, P. Kumar, R. Raman, Corrosion of 2205 duplex stainless steel in chloride medium containing sulfate-reducing bacteria, Electrochim. Acta 52 (2007) 3985–3994.
[2] S.E. Childers, S. Ciufo, D.R. Lovley, *Geobacter metallireducens* accesses insoluble Fe (iii) oxide by chemotaxis, Nature 416 (2002) 767–769.
[3] D. Liu, R. Jia, D. Xu, H. Yang, Y. Zhao, M. saleem Khan, S. Huang, J. Wen, K. Yang, T. Gu, Biofilm inhibition and corrosion resistance of 2205-Cu duplex stainless steel against acid producing bacterium *Acetobacter aceti*, J. Mater. Sci. Technol. 35 (2019) 2494–2502.
[4] R. Jia, J.L. Tan, P. Jin, D.J. Blackwood, D. Xu, T. Gu, Effects of biogenic H2S on the microbiologically influenced corrosion of C1018 carbon steel by sulfate reducing *Desulfovibrio vulgaris* biofilm, Corros. Sci. 130 (2018) 1–11.
[5] E. Zhou, H. Li, C. Yang, J. Wang, D. Xu, D. Zhang, T. Gu, Accelerated corrosion of 2304 duplex stainless steel by marine *Pseudomonas aeruginosa* biofilm, Int. Biodeterior. Biodegrad. 127 (2018) 1–9.
[6] Y. Jin, Z. Li, E. Zhou, Y. Lekbach, D. Xu, S. Jiang, F. Wang, Sharing riboflavin as an electron shuttle enhances the corrosivity of a mixed consortium of *Shewanella oneidensis* and *Bacillus licheniformis* against 316L stainless steel, Electrochim. Acta 316 (2019) 93–104.
[7] D. Xu, W. Huang, G. Ruschau, J. Hornemann, J. Wen, T. Gu, Laboratory investigation of MIC threat due to hydrotest using untreated seawater and subsequent exposure to pipeline fluids with and without SRB spiking, Eng. Fail. Anal. 28 (2013) 149–159.
[8] F. Wang, Y. Gu, J.P. O'Brien, S.M. Yi, S.E. Yalcin, V. Srikanth, C. Shen, D. Vu, N. L. Ing, A.I. Hochbaum, E.H. Egelman, N.S. Malvankar, Structure of microbial nanowires reveals stacked hemes that transport electrons over micrometers, Cell 177 (2019) 361–369.
[9] M. Shao, C. Lin, A review of investigation on pitting corrosion of aluminum alloy, Corros. Sci. Prot. Technol. 14 (2002) 147–151.
[10] Z. Szklarska-Smialowska, Pitting corrosion of aluminum, Corros. Sci. 41 (1999) 1743–1767.
[11] B. Wang, L. Zhang, Y. Su, Y. Xiao, J. Liu, Corrosion behavior of 5A05 aluminum alloy in NaCl solution, Acta Metall. Sin. 26 (2013) 581–587.
[12] A. Rajasekar, Y.P. Ting, Microbial corrosion of aluminum 2024 aeronautical alloy by hydrocarbon degrading bacteria *bacillus cereus ACE4* and *serratia marcescens ACE2*, Ind. Eng. Chem. Res. 49 (2010) 6054–6061.
[13] J. Wang, F. Xiong, H. Liu, T. Zhang, Y. Li, C. Li, W. Xia, H. Wang, H. Liu, Study of the corrosion behavior of *Aspergillus niger* on 7075-T6 aluminum alloy in a high salinity environment, Bioelectrochemistry (2019) 10–17.
[14] F. Guan, J. Duan, X. Zhai, N. Wang, J. Zhang, D. Lu, B. Hou, Interaction between sulfate-reducing bacteria and aluminum alloys—corrosion mechanisms of 5052 and Al-Zn-In-Cd aluminum alloys, J. Mater. Sci. Technol. (2019) 55–64.
[15] F. Guan, X. Zhai, J. Duan, J. Zhang, K. Li, B. Hou, Influence of sulfate-reducing bacteria on the corrosion behavior of 5052 aluminum alloy, Surf. Coat. Technol. 316 (2017) 171–179.
[16] V.F. Smirnov, D.V. Belov, T.N. Sokolova, O.V. Kuzina, V.R. Kartashov, Microbiological corrosion of aluminum alloys, Appl. Biochem. Microbiol. 44 (2008) 192–196.
[17] A. Pedersen, S. Kjelleberg, M. Hermansson, A screening method for bacterial corrosion of metals, J. Microbiol. Methods 8 (1988) 191–198.
[18] G. Gunasekaran, S. Chongdar, S.N. Gaonkar, P. Kumar, Influence of bacteria on film formation inhibiting corrosion, Corros. Sci. 46 (2004) 1953–1967.
[19] A. Jayaraman, E.T. Cheng, J.C. Earthman, T.K. Wood, Axenic aerobic biofilms inhibit corrosion of SAE 1018 steel through oxygen depletion, Appl. Microbiol. Biotechnol. 48 (1997) 11–17.
[20] Z.H. Dong, T. Liu, H.F. Liu, Influence of EPS isolated from thermophilic sulphate-reducing bacteria on carbon steel corrosion, Biofouling 27 (2011) 487–495.
[21] S. Chongdar, G. Gunasekaran, P. Kumar, Corrosion inhibition of mild steel by aerobic biofilm, Electrochim. Acta 50 (2005) 4655–4665.
[22] M. Moradi, Z. Sun, Z. Song, H. Hu, Effect of proteases secreted from a marine isolated bacterium *Bacillus vietnamensis* on the corrosion behaviour of different alloys, Bioelectrochemistry 126 (2019) 64–71.
[23] J. Schmitt, H.C. Flemming, FTIR-spectroscopy in microbial and material analysis, Int. Biodeterior. Biodegrad. 41 (1998) 1–11.
[24] T. Liu, Z. Guo, Z. Zeng, N. Guo, Y. Lei, T. Liu, S. Sun, X. Chang, Y. Yin, X. Wang, Marine bacteria provide lasting anticorrosion activity for steel via biofilm-induced mineralization, ACS Appl. Mater. Interfaces 10 (2018) 40317–40327.
[25] M. Moradi, Z. Song, X. Tao, Introducing a novel bacterium, *Vibrio neocaledonicus* sp., with the highest corrosion inhibition efficiency, Electrochem. Commun. 51 (2015) 64–68.
[26] N. Kip, J.A. van Veen, The dual role of microbes in corrosion, ISME J. 9 (2015) 542–551.
[27] M. Moradi, J. Duan, H. Ashassi-Sorkhabi, X. Luan, De-alloying of 316 stainless steel in the presence of a mixture of metal-oxidizing bacteria, Corros. Sci. 53 (2011) 4282–4290.
[28] J.R. Davis, Corrosion of Aluminum and Aluminum Alloys, ASM International, 1999.
[29] I.B. Beech, J. Sunner, Biocorrosion: towards understanding interactions between biofilms and metals, Curr. Opin. Biotechnol. 15 (2004) 181–186.
[30] X. Sheng, Y.P. Ting, S.O. Pehkonen, The influence of sulphate-reducing bacteria biofilm on the corrosion of stainless steel AISI 316, Corros. Sci. 49 (2007) 2159–2176.
[31] N. Imaz, M. Ostra, M. Vidal, J.A. Díez, M. Sarret, E. García-Lecina, Corrosion behaviour of chromium coatings obtained by direct and reverse pulse plating electrodeposition in NaCl aqueous solution, Corros. Sci. 78 (2014) 251–259.
[32] H. Tsuchiya, S. Fujimoto, O. Chihara, T. Shibata, Semiconductive behavior of passive films formed on pure Cr and Fe–Cr alloys in sulfuric acid solution, Electrochim. Acta 47 (2002) 4357–4366.
[33] X. Qian, N. Gu, Z. Cheng, X. Yang, E. Wang, S. Dong, Impedance study of $(PEO)_{10}LiClO_4$–Al_2O_3 composite polymer electrolyte with blocking electrodes, Electrochim. Acta 46 (2001) 1829–1836.

[34] J.Y. Sha, H.H. Ge, C. Wan, L.T. Wang, S.-Y. Xie, X.J. Meng, Y.Z. Zhao, Corrosion inhibition behaviour of sodium dodecyl benzene sulphonate for brass in an Al_2O_3 nanofluid and simulated cooling water, Corros. Sci. 148 (2019) 123–133.
[35] L. Esteves, C.S. Witharamage, J. Christudasjustus, G. Walunj, S.P. O'Brien, S. Ryu, T. Borkar, R.E. Akans, R.K. Gupta, Corrosion behavior of AA5083 produced by high-energy ball milling, J. Alloys Compd. 857 (2021) 158268.
[36] M. Mehdizade, A.R. Eivani, M. Soltanieh, Effects of reduced surface grain structure and improved particle distribution on pitting corrosion of AA6063 aluminum alloy, J. Alloys Compd. 838 (2020) 155–464.
[37] F. Lappe, L.I. Ljamina, N.I. Korol'kova, The chemical nature of aluminum corrosion, J. Electrochem. Soc. 4 (1982).
[38] K.K. Jefferson, What drives bacteria to produce a biofilm? FEMS Microbiol. Lett. 236 (2004) 163–173.
[39] R. Jia, T. Unsal, D. Xu, Y. Lekbach, T. Gu, Microbiologically influenced corrosion and current mitigation strategies: a state of the art review, Int. Biodeterior. Biodegrad. 137 (2019) 42–58.